




Intelligent Detection of Vegetation Encroachment of Power Lines With Advanced Stereovision

Shuaiang Rong, *Student Member, IEEE*, Lina He , *Member, IEEE*, Liang Du , *Member, IEEE*, Zuyi Li , *Senior Member, IEEE*, and Shiwen Yu

Abstract—Vegetation encroaching on overhead power lines can cause short circuit faults and pose a major threat to the security and stability of power grids. Therefore, establishing an effective visual detection algorithm to oversee potential circuit failures of the power lines is critical to the ongoing inspection of vegetation encroachment. This paper establishes a deep learning-based detection framework that utilizes the images obtained from vision sensors mounted on power transmission towers. The proposed detection framework includes three cascaded modules: (1) detection of vegetation regions based on the Faster Region Convolution Neural Network (Faster R-CNN), (2) detection of power lines based on the Hough transform, and (3) detection of vegetation encroachment based on an advanced stereovision (SV) algorithm. In particular, the proposed SV algorithm converts the detected two-dimensional (2D) image data of the vegetation and power lines to three-dimensional (3D) height and location results in order to obtain precise geographical locations. Case studies using field captured images provided by a Transmission System Operator (TSO) demonstrate the effectiveness of the proposed framework in detecting vegetation failures, thus improving overall reliability and reducing economic loss.

Index Terms—Deep learning, digital image, hough transform, power lines, stereovision, short circuit fault, vegetation management.

I. INTRODUCTION

ECOLOGICAL mismanagement may neglect overgrown forests, which are increasingly primed for wildfires. Vegetation encroachment in power line corridors poses severe threats to the bare conductors of overhead power lines due to vegetation growth and wind conditions [1]. This can result in electrical short circuits in the vicinity where trees contact with transmission lines. As transmission lines usually transfer hundreds of megawatts of power from one tower to another tower that can be hundreds of miles away, the reliability of power transfer greatly relies on the secure and stable operation of transmission lines.

Manuscript received May 20, 2020; revised September 19, 2020 and November 21, 2020; accepted November 22, 2020. Date of publication December 21, 2020; date of current version November 22, 2021. Paper no. TPWRD-00747-2020. (Corresponding author: Lina He.)

Shuaiang Rong, Lina He, and Shiwen Yu are with the Electrical and Computer Engineering Department, University of Illinois at Chicago, Chicago, IL 60607 USA (e-mail: srong4@uic.edu; lhe@uic.edu; syu65@uic.edu).

Liang Du is with the Electrical and Computer Engineering Department, Temple University, Philadelphia, PA 19122 USA (e-mail: ldu@temple.edu).

Zuyi Li is with the Electrical and Computer Engineering Department, Illinois Institute of Technology, Chicago, IL 60616 USA (e-mail: lizu@iit.edu).

Color versions of one or more figures in this article are available at <https://doi.org/10.1109/TPWRD.2020.3043433>.

Digital Object Identifier 10.1109/TPWRD.2020.3043433

With the rapidly increasing consumption of electric power, the operation environment of overhead power lines has become more complex, especially in undeveloped natural areas. The incidents caused by the external conflict between vegetation and overhead lines have become a critical issue of forest management.

Ineffective vegetation management was identified as a major cause of the Northeast Blackout of 2003. This blackout affected an estimated 55 million people in the U.S. and Canada. It also has been a causal factor for 290 automatic North American outages from 2009 to 2016 [2]. To reduce the risk of vegetation-related outages, the North American Electric Reliability Corporation (NERC) developed the vegetation management reliability standard (NERC FAC-003) that defines clearance distances for specific voltage levels of transmission lines [3]. Therefore, it is significant for power utilities to develop effective vegetation management schemes to comply with the standard requirements and avoid potential circuit failures.

The common manual power line inspection with foot patrols and helicopters can be exhaustive and time-consuming [4]. It is also hard to determine the violation of the vegetation clearance distance solely relying on human eyesight from a long distance, thus leading to a high false rate and ignorance on the judgment of vegetation encroachment determination [5]–[6]. As a result, those traditional inspections cannot meet the requirements of the reliable operation of power lines.

The unmanned aerial vehicle (UAV) with light detection and ranging (LiDAR) techniques or digital cameras has been widely applied to improve the efficiency and accuracy of the vegetation encroachment detection [7]. However, the inspection using the UAV with LiDAR requires costly components, e.g., LiDAR sensors and the global positioning system (GPS), and needs to deal with a large amount of computation for data processing [8]. UAVs with cameras apply the stereovision (SV) technology that can generate the 3D information from 2D images based on the parallax of binocular images [9]–[10]. However, the detection results using these aerial imaging methods are usually inaccurate as they use dynamic camera coordinates [11]. Another alternative is to apply the satellite imaging technology with the SV to produce a 3D depth map to measure the vegetation encroachment [12]. However, these aerial imaging-based methods using UAVs or satellites can only distinguish trees based on the color analysis of tree crowns, which does not work when the color of trees changes or is close to their background color [13]. The satellite imaging-based methods also have lower accuracy due to their

low image resolutions [7]. As a result, these vegetation encroachment detection methods cannot provide continuous monitoring with high accuracy and a low cost.

Strategic defense for power infrastructure has been envisioned with grid vulnerability issues and adaptive control mechanisms [14]. Wireless sensor network (WSN) and vision sensors are extensively implemented to monitor power system environments and have been deployed on power towers as part of the transmission monitoring framework [15]–[16]. The deployment of these vision sensors enables continuous monitoring and development of intelligent inspection of vegetation encroachment for power lines [17]. In a large scene of power line corridors, the accuracy of the traditional SV algorithm decreases dramatically [18]–[19]. To adapt and improve the accuracy of SV in a large-scale scene, this paper presents an advanced SV algorithm that incorporates two new optimization subroutines into the traditional SV algorithm.

Recognizing objects in images can be implemented based on the Hough transform algorithm, which can detect power lines accurately and robustly [20]. However, the tree detection in an image is much more complicated from the ground view due to the complex background and ongoing tree morphology. Deep learning techniques have greatly improved the performance of image recognition and provide opportunities to overcome this challenge [21]–[22]. This paper utilizes a deep learning algorithm, i.e., faster regional-convolution neural network (Faster R-CNN) to detect vegetation regions. The Faster R-CNN has been developed to detect the object accurately by providing high-quality region proposals [23]. Combined with the proposed SV module, the location and height information of trees and power lines can be determined in 3D.

The major contribution of this paper is the proposal of the intelligent detection framework of vegetation encroachment, which includes (1) detection of vegetation regions, (2) detection of power lines, and (3) novel stereo vision improvement. This framework integrates the Faster R-CNN and Hough transform into the stereovision algorithm innovatively for the first time to achieve cost-effective monitoring of the vegetation encroachment of power lines. In addition, two optimization subroutines are developed to innovate the traditional stereovision algorithm and improve its accuracy and feasibility in a large-scale scene of power line corridors. The proposed framework can be easily deployed in the monitoring system of power systems by TSOs for the vegetation encroachment inspection. It is also able to provide a cost-effective method for TSOs to comply with the NERC FAC-003. The traditional vegetation inspection methods need a specific budget for each inspection that is required at least once per year [3]. However, using the proposed framework, TSOs only need to invest once to set up the WSN and cameras on power towers surrounded by dense vegetation. The proposed framework can also provide more accurate detection results by providing the actual 3D visualization of a scene with high-resolution images [7]. The effectiveness of the proposed framework is verified with realistic monitoring images from a TSO.

This paper is organized as follows. Section II outlines the proposed framework. Section III introduces the power line detection

module and vegetation detection module. Section IV introduces the principles of the proposed advanced SV module. Section V shows the results of vegetation detection and discusses the effectiveness of the proposed framework. Section VI concludes this paper.

II. OUTLINE OF PROPOSED FRAMEWORK

The proposed online intelligent detection framework is illustrated in Fig. 1. The existing power line image monitoring systems mainly utilize wired equipment such as optical fiber or wireless 4G to send images to the monitoring center. Wireless communication is widely applied in monitoring systems due to its low cost. However, the limitation of the wireless channel bandwidth will affect the quality of images. This cannot meet the requirements of manual visual inspection or automatic recognition [24]. To address this issue, this paper proposes a local image processor that can be embedded with the detection framework. When there is an alarm or a need for real-time viewing, the processor can send images to the monitoring center. This can effectively relieve the burden of wireless communication and ensure image quality.

As shown in Fig. 1, with the binocular vision sensors mounted on a power tower, their image data is collected and processed in the local image processor, where the intelligent vegetation encroachment framework is embedded to detect vegetation and power lines, and identify their 3D height and location information. When the height of a tree violates the clearance distances of power lines, the local processor sends an alarm to the monitoring center to assign a maintenance crew to trim the tree. The image data is processed by the deep learning-based detection module and the Hough transform-based module to detect trees and power lines, respectively. The detection results are then processed by the proposed advanced SV model. As a result, 2D information of the trees and power lines in images are converted to the 3D information and their heights are determined.

Fig. 2 shows the flowchart of the intelligent detection framework consisting of three parts: 1) detection of trees and power lines, 2) 3D reconstruction using stereovision, and 3) vegetation encroachment determination.

Step 1. Detection of power lines and trees: In order to determine the 3D information of trees and power lines, their shapes and positions in 2D images need to be identified. The power lines are detected with the developed power line detection module including a straight-line detection tool, i.e., the Hough transform algorithm. The trees are difficult to detect due to their complex and various morphologies, e.g., colors and shapes. Therefore, the Faster R-CNN is first used in this paper to detect trees for vegetation detection, as in Fig. 2.

Step 2. Stereovision: After trees and power lines are detected in 2D images, their 3D information can be calculated by applying the SV algorithm. The traditional SV algorithm cannot be applied to the power line monitoring directly due to its bad performance in large-scale scenes with complex backgrounds [19]. Therefore, an advanced SV algorithm is proposed to adapt the traditional SV algorithm by incorporating new optimization subroutines.

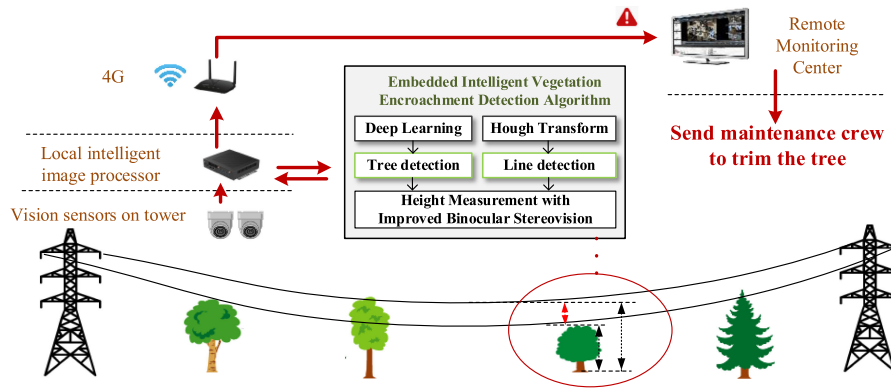


Fig. 1. Detection of vegetation encroachment in power line corridor.

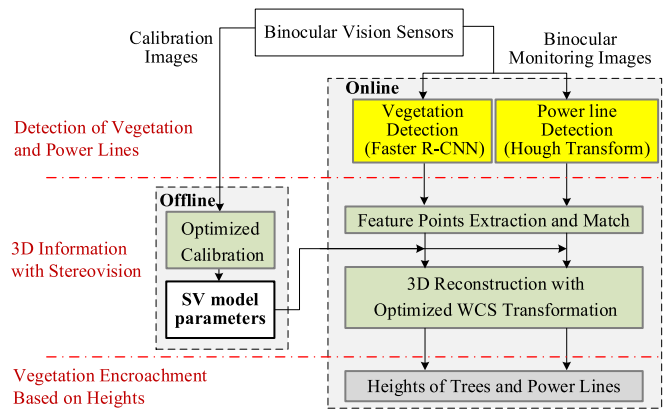


Fig. 2. Flowchart of proposed vegetation encroachment detection framework.

- 1) *Optimized Calibration.* Camera calibration is an offline process that establishes an SV model to represent the relationship of 2D images and 3D space by calculating the intrinsic and extrinsic parameters of binocular cameras. The parameters are calculated based on Zhang's calibration method with the known geometry information of a plane and its projection image coordinates on binocular images [18]. To improve the accuracy of the calibration, an optimization subroutine is proposed to perform the calibration iteratively.
- 2) *Feature Points Extraction and Match.* The 3D information of trees and power lines rely on the 3D coordinates of their feature points, which can be calculated from their 2D image coordinates in the binocular images using the established SV model. Therefore, the feature points of trees and power lines in binocular images need to be extracted and matched to calculate their 3D coordinates.
- 3) *3D Reconstruction.* The determination of 3D coordinates of feature points is defined as 3D reconstruction. To optimize this process, an optimization algorithm is developed to transform the reconstructed world coordinate system (WCS) to a ground-based coordinate system (GCS). This allows the direct height measurement of power lines and

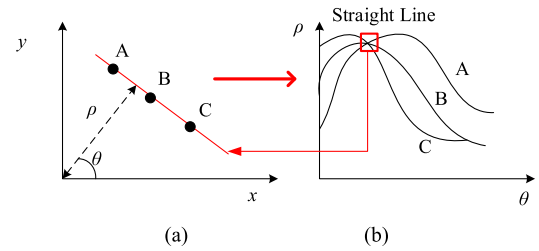


Fig. 3. Straight-line detection in images using Hough Transform. (a) Image (b) Hough space.

trees in a 3D coordinate system based on the real-world ground.

Step 3. Vegetation encroachment determination: Based on the heights and locations of power lines and trees, their height gap (i.e., vegetation encroachment) can be determined. If the vegetation encroachment violates the clearance distance, an alarm signal will be sent to the remote monitoring center to trigger maintenance work for the mitigation.

III. DETECTION OF POWER LINES AND VEGETATION

During online monitoring, binocular images are obtained and applied to the detection of power lines and trees.

A. Detection of the Line Object

The power lines are detected using Hough transform, which transforms the coordinates of pixels in images to the curves in a Hough space, as in Fig. 3 [25].

The principle of line detection is introduced as follows. In the Hough space, a straight line is represented as,

$$\rho = x \times \cos \theta + y \times \sin \theta \quad (1)$$

where coordinates (x, y) are the image coordinates of a pixel. The symbol θ represents the angle of the line inclination to the x -axis. The symbol ρ represents the perpendicular distance from the origin to the line. As shown in Fig. 3, each pixel (e.g., A, B, and C) in an image has a corresponding value of ρ with varied θ , and can be converted to a curve in the Hough space.

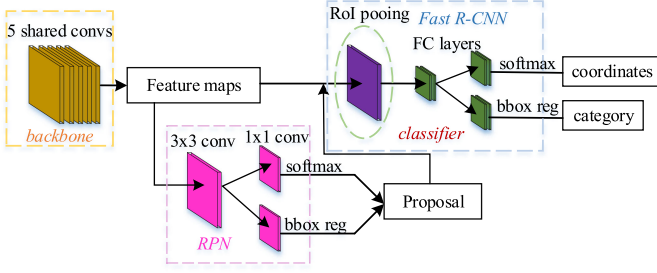


Fig. 4. Structure of Faster R-CNN.

Therefore, the straight line across points A, B, and C in the image is determined by the intersection of curves A, B, and C.

B. Deep Learning-Based Vegetation Detection

To detect vegetation in images, a neural network based on the Faster R-CNN is designed and trained to generate the bounding boxes (represented as bboxes in the following content) of vegetation regions. The Faster R-CNN includes the region proposal network (RPN) and Fast R-CNN. The RPN predicts the regions by determining the probability of the region containing a target object and generates region proposals, which are then applied to the Fast R-CNN block for object recognition and detection. The RPN and Fast R-CNN are merged into a single network by sharing convolutional features in the convolution layers, as shown in Fig. 4.

In the process, binocular images are fed to the shared convolution layers to exact feature maps, which are shared with the subsequent RPN and fully connected (FC) layers. In the RPN, a softmax layer is used to identify region proposals containing the target object, and the bbox regression layer is used to modify regions to obtain accurate proposals. The region of interest (RoI) pooling layer collects the input feature maps and proposals, extracts the proposed feature maps, and sends them to the FC layers in the Fast R-CNN. As a result, the categories and positions of bboxes are obtained from the softmax and bbox regression layers, respectively.

This paper develops a CNN consisting of three parts: 1) an image input layer to restrict the type and size of the input images; 2) 3 convolutional layers, each has 32.5×5 filters and is followed by a rectified linear unit (ReLU) layer and a pooling layer, are used in the middle part to extract feature maps; 3) FC layers with 64 neurons and a softmax loss layer to identify the desired region proposals containing the target objects. The CNN is pre-trained with the CIFAR-10 database including 50,000 images with a small size (i.e., 32×32 pixels) [26]. This can reduce the training time on a limited graphic processing unit (GPU).

IV. ADVANCED STEREOVISION MODULE

After trees and power lines are detected in the 2D images, their 3D information can be determined by applying the advanced SV module proposed in this section.

Calibration Optimization Algorithm

Result: Optimal SV parameters with identical focal lengths

Step 1: Obtain initial focal lengths of cameras 1 and 2 represented by symbols $f_{l,1}$ and $f_{r,1}$ via the first iteration of calibration

Step 2: Initialize scale factor $k_1 \leftarrow 1$, $k_2 \leftarrow f_{l,1}/f_{r,1}$, iteration time $i \leftarrow 2$ and regulating factor $\beta \leftarrow 2$

Step 3: Find the optimal value of scale factor minimizing the difference of focal lengths:

While ($|f_{l,i} - f_{r,i}| > 1$) **do**

Step 3.1: Update the calibration with coordinates of the calibration points in image 2 multiplying k_i ;

Step 3.2: $\{K_1, \dots, K_n\} \leftarrow$ ascending order of values of $\{k_1, \dots, k_i\}$

Step 3.2: Do following

if ($f_{l,i} \geq f_{r,i}$) **then**

if ($k_i = k_n$) **then**

$k_{i+1} \leftarrow \beta(k_n - 1) + 1$

else

$k_{i+1} \leftarrow (k_n + k_{n-1})/2$

end

else

$k_{i+1} \leftarrow (k_n + k_{n-1})/2$

end

$i \leftarrow i + 1$

end

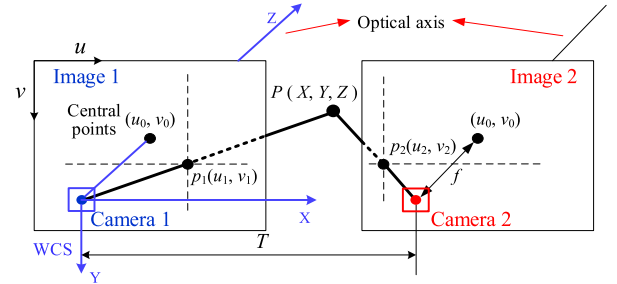


Fig. 5. Ideal SV projection model.

A. Traditional SV Model

The traditional SV is introduced using the ideal parallel SV model to show the necessity of the proposed algorithms. Fig. 5 shows the ideal model with a projection of an object (P) from 3D space to 2D images (p_1 and p_2) [18]. The optical axes of binocular cameras are assumed parallel, and intrinsic parameters of the binocular cameras are assumed identical. Based on the optical geometric law, 3D coordinates of the point P in WCS can be represented by the intrinsic and extrinsic parameters, along with projected image coordinates of points p_1 and p_2 , as in (2),

$$X = \frac{T}{T-d} (u_1 - u_0), Y = \frac{T}{T-d} (v_1 - v_0) \alpha, Z = \frac{Tf}{T-d} d = [(u_0 - u_2) - (u_1 - u_0)] \alpha = (u_1 - u_2) \alpha \quad (2)$$

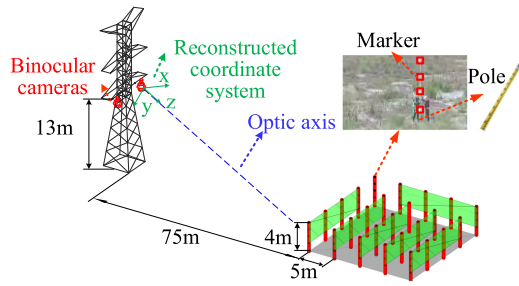


Fig. 6. Experiment set-up for binocular camera calibration.

where the symbol d represents the parallax, (X, Y, Z) are the 3D coordinates of P , (u_1, v_1) and (u_2, v_2) are the 2D image pixel coordinates of the projection (p_1 and p_2) in images 1 and 2, respectively. The intrinsic parameters include 1) image pixel coordinates of image central points represented by the coordinates (u_0, v_0) ; 2) the pixel physical length represented by symbol α ; 3) the focal length represented by symbol f . The extrinsic SV parameters include the translation vector (represented by symbol T), and the rotation matrix between the binocular images (which is a unit matrix in this case).

Based on this model, the parameters can be calculated via calibration with the known image coordinates and the 3D world coordinates of the calibration points. The reconstruction is the reverse process of the projection, which is to determine the 3D coordinates from its matched coordinates in binocular images and parameters determined via calibration.

B. Field Set-Up for Camera Calibration

The camera calibration is to determine binocular camera parameters with the known geometry data of calibration objects in the field images. A calibration object is usually a checkerboard-like plane, which, however, is not practical to be used in a power line corridor due to the large area [18]. A pole ruler is adopted as a calibration object to expand the calibration area, as in Fig. 6.

The pole is 4 meters and placed on the field ground vertically tied with a white marker at each meter, which can be extracted as calibration points. The pole is placed transversely and longitudinally every 5 meters to form a matrix comprising 6 calibration planes shown as green in Fig. 6. With the 2D image coordinates of extracted calibration points, the intrinsic and extrinsic parameters are calculated. It is noted that the WCS is based on the coordinate system of camera 1 in the traditional SV model, as defined in Fig. 5.

The binocular sensors are Pan/Tilt/Zoom (PTZ) cameras, whose positioning can be controlled and recorded remotely. After calibration, the generated SV parameters and position information can be saved for applications in new sites.

C. Calibration Optimization of Advanced SV

The assumption of identical intrinsic parameters of binocular cameras in the traditional SV model ensures high accuracy of the calibration [18]. Therefore, the traditional SV generally uses the same product for binocular cameras with a fixed-focal

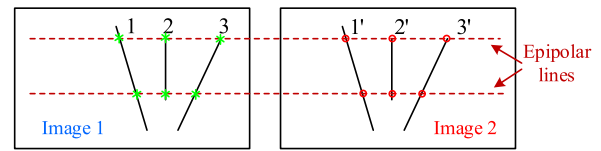


Fig. 7. The power line detection with epipolar constraints.

length. This assumption is, however, challenged by zoomable surveillance cameras with changeable focal length settings of a low precision applied in power line corridors. The resulting focal length gap of binocular cameras can cause a significant error in the calibration.

To eliminate this error, an optimization subroutine is proposed to regulate the focal length of camera 2 to be identical to the focal length of camera 1 by changing its image coordinates. As shown in the chart of the algorithm, Steps 1 and 2 initialize the focal lengths, the scale factor, and the regulating factor that is used to change the calibration coordinates of image 2. Step 3.2 shows the optimization process of the scale factor that minimizes the focal length gap of two cameras obtained via the calibration. Specifically, when the focal length of image 1 is larger (smaller) than that of image 2, the scale factor will increase (decrease) for next step process. The regulating factor is a constant value (set as 2). It determines the increment of the scale factor when the current scale factor is the largest value in all the previous iterations. Otherwise, the increased or decreased scale factor adopts the middle value between the previous value and its adjacent value.

D. Feature Extraction and Match of Advanced SV

To calculate 3D information of power lines and trees, their feature points in the images need to be extracted and matched to calculate the parallax. Due to their different characteristics, this process is achieved by two distinct methods.

The feature points of trees are extracted using the scale invariant feature transform (SIFT) algorithm, which is a feature detection algorithm to detect local features (e.g., the texture and color) in images [27]. These points in binocular images can be matched in pairs if they have the same features. However, feature points on a power line are difficult to extract and match, as they all have the same texture and color. To address this issue, a new method based on the epipolar constraints is developed. Using the parameters of the proposed advanced SV model, the image distortion and angle differences of the binocular images can be eliminated through image rectification. It allows the corresponding feature points in the binocular images to be at the same horizontal level (i.e., an epipolar line), which is defined as epipolar constraints [18]. The corresponding points on the power lines can be determined with the intersection of the epipolar lines, as shown in Fig. 7. As a result, the feature points in image 1 (points 1, 2, 3) and in image 2 (points 1', 2', 3') are determined and matched by the intersection between the power lines and the epipolar lines.

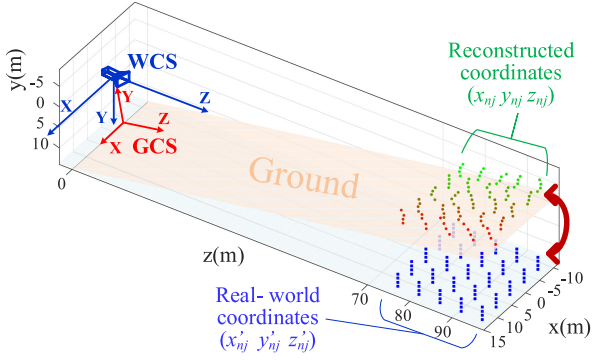


Fig. 8. Transformation from WCS to GCS for constructed 3D coordinates.

E. WCS Transformation of Advanced SV

With coordinates of the matched points, the 3D coordinates are reconstructed with the parameters of the advanced SV model. In the traditional SV algorithm, the reconstructed 3D coordinates of feature points are in a WCS, which is based on the coordinate system of the camera 1. The WCS is not practical for height measurement as it has no correlation with the real-world field ground. To resolve this issue, the WCS is regulated to a GCS based on an optimization problem, which aims to find the transformation matrix between the 3D reconstructed coordinates and 3D real-world calibration coordinates from field measurements, as shown in Fig. 8.

Since axes X, Y, Z of the WCS are determined by the arbitrary position and angle of the camera 1, the reconstructed calibration points aligned by the real-world ground are not related to the X-Z plane in the WCS. The transformation enables the ground in WCS to be on the X-Z plane of the GCS so that heights can be determined accurately by reconstructed coordinates. The transformation can be represented by (3),

$$\begin{bmatrix} x_{nj}^r & y_{nj}^r & z_{nj}^r & 1 \end{bmatrix}^T = \begin{bmatrix} x_{nj} & y_{nj} & z_{nj} & 1 \end{bmatrix}^T R_1 R_2 R_3 \quad (3)$$

where the coordinates $[x_{nj} \ y_{nj} \ z_{nj} \ 1]^T$ are the homogeneous coordinates of the j_{th} top point of the n_{th} pole, the coordinates $[x_{nj}^r \ y_{nj}^r \ z_{nj}^r \ 1]^T$ are homogeneous coordinates after transformation. Symbols R_1, R_2, R_3 are transformation matrixes composed of the angles in X/Y/Z direction. The goal of this algorithm is to find the transformation matrixes that minimize the difference between reconstructed coordinates and real-world coordinates. The objective function is the average standard deviation (ASD) of 4 points on the n_{th} pole represented by symbol H_n , as presented in (4).

$$H_n = \frac{1}{2} \sqrt{\sum_{j=1}^4 (x_{nj}^r - x'_{nj})^2 + (y_{nj}^r - y'_{nj})^2 + (z_{nj}^r - z'_{nj})^2} \quad (4)$$

where $(x'_{nj} \ y'_{nj} \ z'_{nj})$ are corresponding coordinates in real-world coordinates based on GCS. To find the global optimal solution, the optimization problem is described as a Chebyshev approximation problem, which is to find the minimum value of the maximum element in a set [28]. The objective function is shown in (5), the decision variables are the angles in the

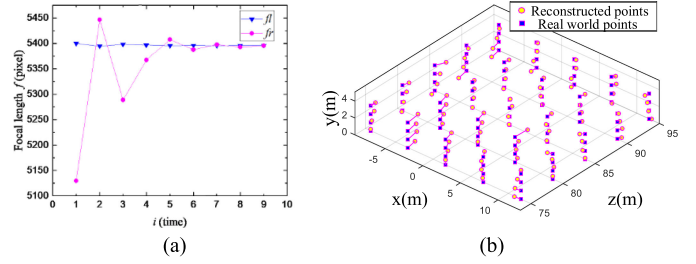


Fig. 9. Results of optimization subroutines: (a) focal lengths during calibration optimization, and (b) reconstructed points with optimal calibration in GCS.

transformation matrix,

$$\text{minimize } H_m = \max\{H_1, \dots, H_n\} \quad (n = 1, \dots, 25) \quad (5)$$

The optimal solution of the transformation matrix can be determined using the quasi-Newton method [28]. Applying the transformation matrix, the 3D reconstruction of the feature points of power lines and trees can be put into a GCS, which can directly provide the height information.

V. CASE STUDIES AND DISCUSSION

The optimization of the calibration and the transformation of WCS are verified to prove the effectiveness of the advanced SV module. Case studies are carried out to demonstrate the effectiveness of the proposed framework based on the realistic test images from a TSO. The 3D height and location information of trees and power lines in the realistic testing images are reported in this section.

A. Optimization of Calibration and WCS Transformation

In the optimization of the calibration, the calculated focal lengths in the results of calibrations are shown in Fig. 9(a). It shows that the focal length f_r of camera 2 gradually converges to the focal length f_l of camera 1 after 9 iterations.

After the transformation, the reconstructed coordinate system WCS is transformed into a GCS. The comparison of the reconstructed coordinates with the real-world coordinates of calibration points is shown in Fig. 9(b). Comparing with Fig. 8, the reconstruction points floating on the WCS are now on the X-Z plane (ground) and are very close to real-world coordinates in the GCS, which shows the effectiveness of the transformation. In addition, the reconstructed points in Fig. 9(b) use the optimal calibration parameters. Using the optimal calibration parameters, the maximum ASD (H_m) between the reconstructed and real-world coordinates of the calibration points on poles in equation (5) is reduced from 3.04 m to 0.27m, which has a reduction of 91.1%. This indicates that the difference of 3D reconstruction coordinates and the real-world coordinates of calibration points is further reduced, which shows that the accuracy of the reconstruction is improved. The reduced ASD also indicates that the proposed framework is applicable for 3D reconstruction of objects that are within a range from the power tower to 95 m with high accuracy.

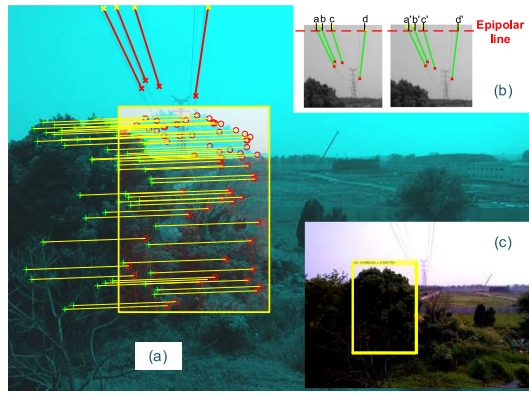


Fig. 10. Case 1: (a) Feature extraction and matching of the tree and line detection and (b) Epipolar constraints (c) Tree detection bbox.

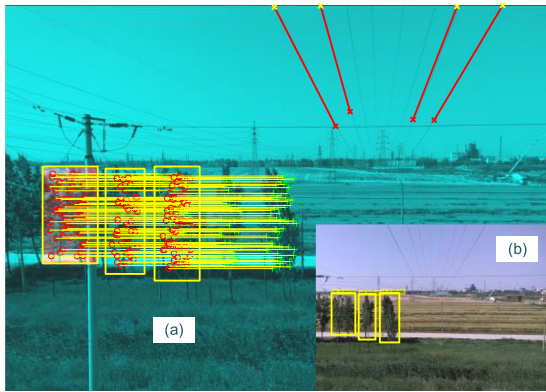


Fig. 11. Case 2: (a) Feature extraction and matching of the tree and line detection and (b) Tree detection bboxes.

B. Vegetation Encroachment Detection

The proposed framework is tested by two cases of transmission line sites with voltage levels of 500 kV and 220 kV. Their detection results of power lines and vegetation are shown in Fig. 10 and Fig. 11. In both cases, the binocular cameras are pre-calibrated and mounted on a tower with the height of 13 m from the ground. They are 2 m away from each other. The vegetation in the images is about 30 m away from the tower. As shown in Fig. 10 (a) and Fig. 11 (a), four power lines are successfully detected in the binocular images in each case. Fig. 10 (b) shows the epipolar constraints for the height measurement of power lines. An epipolar line is set to generate the corresponding points a (a'), b (b'), c (c'), and d (d'). Using the same method, the corresponding points of power lines in case 2 are also determined. The calculated 3D coordinates of these points are shown in Table I. The Y coordinate gives the heights of the points on the power lines.

A Faster R-CNN detector is developed via training to detect vegetation for test cases. A neural network is trained using the datasets consisting of 70 images of trees with different shapes in flourishing and withering conditions. Afterwards, the neural network is tested via 20 tree images. The testing results show the trees of 95% in 20 images are successfully detected with bboxes.

TABLE I
MEASUREMENTS OF POWER LINES

Points	Case 1			Case 2		
	3D coordinates (m)			3D coordinates (m)		
	X	Y	Z	X	Y	Z
a	-2.36	16.92	28.93	1.88	15.13	34.20
b	-1.43	17.57	32.11	4.36	15.69	35.02
c	-1.59	18.14	36.74	9.54	15.52	34.23
d	2.55	17.74	32.93	13.51	15.55	34.37

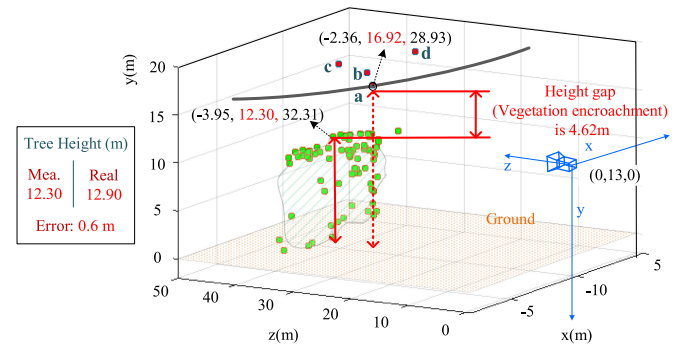


Fig. 12. Measurement results of case 1.

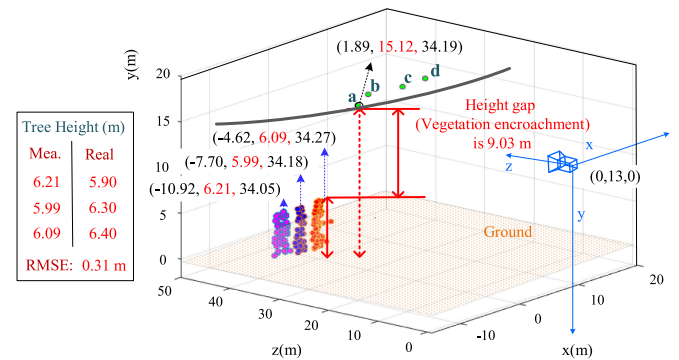


Fig. 13. Measurement results of case 2 (RMSE: Root-Mean-Squared Error).

Applying the detector, one tree is detected in case 1, and three trees are detected in case 2 with bboxes, as shown in Fig. 10 (c) and Fig. 11 (b). The SIFT algorithm extracts and matches all the feature points of the binocular images for 3D reconstruction, as shown in the overlapped binocular images in Fig. 10 (a) and Fig. 11 (a).

The vegetation encroachment detection results are shown in Fig. 12 and Fig. 13, where the 3D reconstruction of points (a, b, c, and d) on power lines and feature points of the trees are drawn based on their 3D coordinates. The Y coordinate of the highest feature point of the trees indicates the height of the trees away from the ground in the coordinate system. The height measurements of the trees in cases 1 and 2 along with their errors are shown in Fig. 12 and Fig. 13, respectively. Based on the four data sets of measurements of the trees and their real heights in both cases (one set of data in Fig. 12 and three sets of data in Fig. 13), the overall root-mean-squared error of their

height measurements can be calculated as 0.40 m. This can meet the actual application requirements of height measurements in a large-scale scene of power line corridors that are usually hundreds of meters. As in Table I, point *a* is the lowest point of the power lines in both cases and their heights are 16.92 m and 15.13 m, respectively. The vegetation encroachment is determined based on the height gap between the power line and vegetation. The height gap is 4.62 m in case 1 and 9.03 m in case 2. Both results don't violate the minimum clearance distances of 500 kV and 230 kV lines in the NERC standard (i.e., 2.13 m and 1.22 m), respectively [3]. In addition to the tree growth, contacts between power lines and vegetation can be also resulted due to an increased line sag caused by load increases or snow. To accommodate these situations, vegetation clearance distance standards of utilities usually adopt larger values, which are usually in the range of 2 m to 3 m for transmission lines in voltage levels from 230 kV to 500 kV in the U.S. [29]. Since the vegetation encroachment results do not violate these requirements as well, there is no alarm and maintenance work triggered in both cases.

This monitoring system is able to be deployed in the power line corridors in terrains with elevation fluctuation, such as hills and valleys, since the vegetation encroachment is determined solely based on the height gap between the power line and vegetation in a coordinate system that is regulated based on a horizontal datum (the virtual ground in GCS).

C. Cost-Effectiveness and Viability of Proposed System

The traditional manned helicopter inspection costs an average of \$870/km for each inspection that is required at least once per year by NERC [3], [30]. Applying the proposed stereovision system, ten cameras are needed per kilometer if considering a case in which five power towers are set with an average spacing of 200 m. The required surveillance camera in the market costs \$250 on average and can easily function for ten years with basic maintenances [31]. Hence, the total cost of the proposed system is \$250/km/year, which is much less than the cost of the traditional method \$870/km/year [30]. With consideration of annual inspections, the proposed system has a slightly higher cost compared with the currently widely researched UAV inspection method that has an average cost of \$156/km/year [30]. However, the proposed system allows constant surveillance, which can bring down the cost of the proposed system to be much less than the UAV inspection for frequent inspections that are required for areas with dense vegetation. For example, the cost of the proposed system will be \$125/km for a semi-annual inspection and only \$20.8/km for a monthly inspection.

VI. CONCLUSION

An intelligent detection framework is proposed in this paper to detect the vegetation encroachment of transmission lines based on the image data monitored from towers with mounted binocular vision sensors. This framework includes the deep learning-based tree detection algorithm, the Hough transform-based power line detection algorithm, and the novel advanced

SV algorithm. Their effectiveness is verified via a case study based on the monitoring data from a TSO.

The results of the case study show that 1) the vegetation detection is achieved with the deep learning-based module, i.e., Faster R-CNN, 2) the power lines are effectively detected with the Hough transform-based module, 3) the height measurement of trees and power lines for the vegetation encroachment detection is achieved, and 4) the accurate localization in geography is also achieved. The proposed framework provides an accurate, cost-effective, and practical vegetation detection methodology, which can provide early warning services for the vegetation management of utilities to avoid potential contacts of vegetation and power lines.

VI. REFERENCES

- [1] S. D. Anagnostatos, C. D. Halevidis, A. D. Polykrati, E. I. Koufakis, and P. D. Bourkas, "High-voltage lines in fire environment," *IEEE Trans. Power Del.*, vol. 26, no. 3, pp. 2053–2054, Jul. 2011.
- [2] H. Gugel *et al.*, "Vegetation-related outages on transmission lines in north america," in *Proc. IEEE Power Energy Soc. Gen. Meeting*, Portland, OR, 2018, pp. 1–5.
- [3] *Transmission Vegetation Management*, NERC Standard FAC-003-4, 2016.
- [4] L. F. Luque-Vega *et al.*, "Power line inspection via an unmanned aerial system based on the quadrotor helicopter," in *Proc. IEEE Mediterranean Electrotech. Conf.*, 2014, pp. 393–397.
- [5] S. Ashidate, S. Murashima, and N. Fujii, "Development of a helicopter-mounted eye-safe laser radar system for distance measurement between power transmission lines and nearby trees," *IEEE Trans. Power Del.*, vol. 17, no. 2, pp. 644–648, Apr. 2002.
- [6] J. Ahmad *et al.*, "Vegetation encroachment monitoring for transmission lines right-of-ways: A survey," *Elect. Power Syst. Res.*, vol. 95, pp. 339–352, Feb. 2013.
- [7] K. Sikorska-Lukasiewicz, "Methods of automatic vegetation encroachment detection for high voltage power lines," in *Proc. SPIE Radioelectron. syst. Conf.*, Jachranka, Poland, Feb. 2020.
- [8] B. Kurinsky and M. Hung, "Identification and visualization of vegetation encroachments along power line corridors using LiDAR," *Int. J. Res. Geogr.*, vol. 1, no. 1, pp. 38–51, Jun. 2015.
- [9] C. Shuai *et al.*, "Power lines extraction and distance measurement from binocular aerial images for power lines inspection using UAV," in *Proc. Int. Conf. Intell. Hum.-Mach. Syst. Cyber.*, Hangzhou, China, 2017, pp. 69–74.
- [10] Q. Li *et al.*, "Bionic vision-based intelligent power line inspection system," *Comput. Math. Methods Med.*, vol. 2017, 2017.
- [11] A. Babineca and J. Apeltauerb, "On accuracy of position estimation from aerial imagery captured by low-flying UAVs," *Int. J. Trans. Sci. Tech.*, vol. 5, no. 3, pp. 152–166, Oct. 2016.
- [12] A. Qayyum *et al.*, "Monitoring of vegetation near power lines based on dynamic programming using satellite stereo images," in *Proc. IEEE Int. Conf. Smart Instrum. Meas. Appl.*, 2014, pp. 1–6.
- [13] L. He *et al.*, "Research on tree crown segmentation method in tree height image monitoring of transmission lines," in *Proc. IEEE Conf. Energy Internet Energy Syst. Integration*, 2019, pp. 2241–2245.
- [14] H. Li, G. Rosenwald, J. Jung, and C.-C. Liu, "Strategic power infrastructure defense," *Proc. IEEE*, vol. 93, no. 5, pp. 918–933, May 2005.
- [15] N. Cottini, L. Gasparini, M. De Nicola, N. Massari, and M. Gottardi, "A CMOS ultra-low power vision sensor with image compression and embedded event-driven energy-management," *IEEE J. Emerg. Sel. Top. Circuits Syst.*, vol. 1, no. 3, pp. 299–307, Sep. 2011.
- [16] B. Fateh, M. Govindarasu, and V. Ajjarapu, "Wireless network design for transmission line monitoring in smart grid," *IEEE Trans. Smart Grid*, vol. 4, no. 2, pp. 1076–1086, Jun. 2013.
- [17] "Future inspection of overhead transmission lines," Electric Power Res. Inst., Palo Alto, CA, U.S., Rep. 1016921, 2008.
- [18] M. Songde and Z. Zhengyou, *Computer Vision—Computational Theory and Algorithmic Basis*. Beijing, China: Science Press, 1998.
- [19] D. Scribner and J. Gombash, "The effect of stereoscopic and wide field of view conditions on teleoperator performance," Army Res. Lab., MD, USA, Rep. ARL-TR-1598, Mar. 1998.

- [20] L. Baker *et al.*, “Power line detection using hough transform and line tracing techniques,” in *Proc. Int. Conf. Image Vision Comput.*, 2016, pp. 1–6.
- [21] V. Nguyen, R. Jenssen, and D. Roverso, “Automatic autonomous vision-based transmission line inspection: A review of current status and the potential role of deep learning,” *Int. J. Elect. Power Energy Syst.*, vol. 99, pp. 107–120, 2018.
- [22] M. Onishi and T. Ise, “Automatic classification of trees using a UAV onboard camera and deep learning,” 2018. [Online]. Available: <https://arxiv.org/abs/1804.10390>
- [23] S. Ren *et al.*, “Faster R-CNN: Towards real-time object detection with region proposal networks,” in *Proc. Neural Inf. Process. Syst. Conf.*, 2015, pp. 91–99.
- [24] Z. Le, W. Liu, and W. Zhao, “Embedded system based invader detection for high-voltage transmission line,” *East China Electric Power*, vol. 42, no. 1, pp. 61–66, 2014.
- [25] R. Duda and P. Hart, “Use of the hough transformation to detect lines and curves in pictures,” *Commun. Assoc. Comput. Machinery*, vol. 15, no. 1, pp. 11–15, Jan. 1972.
- [26] A. Krizhevsky, “Learning multiple layers of features from tiny images,” M.S. thesis, Dept. Comput. Sci., Univ. Toronto, Canada, 2009.
- [27] D. G. Lowe, “Object recognition from local scale-invariant features,” in *Proc. Int. Conf. Comput. Vis.*, 1999, pp. 1150–1157.
- [28] S. Boyd and L. Vandenberghe, *Convex Optimization*. Cambridge, U.K.: Cambridge Univ. Press, 2004.
- [29] *Requirements for All Lines—vegetation Management*, California Public Utilities Commission General Order 95–Rule 35, Jan. 2012.
- [30] T. Mason, “Xcel energy launches drones for power line inspections with a twist,” in *Proc. Columbia Broadcast. Syst.*, Denver, CO, U. S., Sep. 2018.
- [31] Product brochure: DS-2DE4220IW-D, Network IR PTZ Dome Camera, Hikvision Digital Technology Co., Hangzhou. 2016. [Online]. Available: <http://www.akatos.net/ProductPDF/DS-2DE4220IWD.pdf>

Shuaiang Rong (Student Member, IEEE) received the M.S. degree in electric engineering from the Shanghai University of Electric Power, in 2018. She is currently working toward the Ph.D. degree with the University of Illinois, Chicago. Her research interest includes machine learning, image processing, renewable energy integration, and power system protection.

Lina He (Member, IEEE) received the Ph.D. degree in electrical engineering from University College Dublin, Ireland, in 2014. She is currently an Assistant Professor with the Department of Electrical and Computer Engineering, University of Illinois, Chicago. From 2014 to 2017, she was a Project Manager and Senior Consultant with Siemens Headquarter, Germany and Siemens, U.S. Her research interests include modeling, protection, and security of power electronics based power systems, power system operation, and image processing.

Liang Du (Member, IEEE) received the Ph.D. degree in electric energy from the Georgia Institute of Technology, in 2013. He is currently an Assistant Professor with Temple University. His research interests include power grid modernization, data-driven analytics, and renewable integration.

Zuyi Li (Senior Member, IEEE) received the Ph.D. degree in electrical engineering from the Illinois Institute of Technology (IIT), Chicago, in 2002. He is currently a Professor with Electrical and Computer Engineering Department and the Associate Director with the Robert W. Galvin Center for Electricity Innovation, IIT. His research interests include economic and secure operation of electric power systems, cyber security in smart grid, renewable energy integration, and power system protection.

Shiwen Yu received the M.S. degree in electrical engineering from the Wuhan University of Technology, in 2020. He is currently working toward the Ph.D. degree with the University of Illinois, Chicago. His research interests include renewable energy integration, risk assessment, and machine learning.